AIMS Energy, 9(4): 830–841.
DOI: 10.3934/energy.2021038
Received: 31 May 2021
Accepted: 21 June 2021
Published: 28 June 2021

http://www.aimspress.com/journal/energy

Research article

Effect of Ag NPs on the radiant absorption of photocatalyst film

Jiayu Li* and Jiewen Guo

MIIT Key Laboratory of Thermal Control of Electronic Equipment, School of Energy and Power Engineering, Nanjing University of Science and Technology, Nanjing 210094, China

* **Correspondence:** Email: lijiayu@mail.njust.edu.cn; Tel: +15051807486.

Abstract: A composite film composed of Ag nanoparticles, Al_2O_3 and TiO_2 was prepared by cosputtering. Ag NPs were immersed in the Al_2O_3 host, TiO_2 was deposited onto the Ag/Al_2O_3 layer. The degradation of aqueous methylene blue under incident irradiation indicated that the Ag/Al_2O_3-TiO_2 composite film with the Ag-TiO_2 distance of 2nm or 5nm exhibited high degradation rate. Spectral absorptivity and radiant absorption distribution were analyzed through FDTD simulation to analyze the relationship between radiant absorption and photocatalytic activity. Results indicated that the spectrum and distribution of the radiant absorption in the composite film could be rationally regulated to improve photocatalytic activity.

Keywords: Ag nanoparticle; localized surface plasmon resonance; spectral absorptivity; absorption distribution; FDTD simulation; plasmonic photocatalyst

1. Introduction

Noble metal nanoparticles (NPs), such as Ag, Au, and Pt, can harvest visible light effectively due to their Localized Surface Plasmon Resonance (LSPR). Incident irradiation is highly localized at NPs. Generated electrons and holes are efficiently separated at the metal-semiconductor interface due to Fermi level equilibration [1,2]. These properties can be applied for photocatalytic activity. Thus, noble metal NPs are combined with photocatalysts to form plasmonic photocatalysts [3,4]. As the radiant absorption of photocatalyst is the precondition for the photocatalysis reaction, it is necessary to investigate the radiative properties, including the spectral absorptivity and internal radiant absorption, for plasmonic photocatalysts. The simulated research in Ref. [5] have provided a comprehensive analysis for the radiative properties of hedgehog-like ZnO-Au composite particles, their particle models were established based on discrete dipole approximation (DDA) and the

optimized morphology was summarized for the application of photocatalysis. Considering some assumptions and simplifications of the model, they have also developed experimental measurement for the hedgehog-like ZnO-Au composite particles [6].

It is reported that the Ag NPs in the Ag/TiO_2 system would undergo corrosion or dissolution during photocatalytic reaction [7,8]. Thus, a thin insulating shell is employed to protect the Ag NPs. Different types of insulating oxides are suggested, but electron transfer from metal NPs to the insulating shell does not occur [9,10]. When the charge carriers generated by LSPR-induced electromagnetic field are localized to the vicinity of the metal NPs, they cannot migrate to the active sites near photocatalyst surface, so the photocatalytic efficiency is just enhanced by the localized irradiation. Alumina (Al_2O_3) is an earth-abundant and stable metal oxide, which has been widely applied as a supporter for photocatalyst due to its low cost, chemical inertness and efficient photoinduced electron-hole separation [11–13]. In addition, dual layers composed of Al_2O_3 and TiO_2 have been experimentally proven to suppress the recombination rate of electron and hole pairs [14]. From the aspect of incident radiant absorption, the imaginary component of the Al_2O_3 dielectric constant is nearly zero at the wavelengths between 300 nm and 900 nm. Thus, Al_2O_3 can be considered as transparent for the incident irradiation in this wavelength region. So Al_2O_3 was chosen to protect the metal NPs from corrosion for designing and preparing stable and efficient plasmonic photocatalysts. Titanium dioxide (TiO_2) is a sustainable candidate material for photocatalysts due to its good stability, nontoxicity, high efficiency and low cost [15]. The band gap of anatase TiO_2 is 3.2 eV. This characteristic indicates that electrons and holes can be generated in anatase TiO_2 when the wavelength of incident radiation is less than 387.5 nm. The generated carriers can be used for catalytic reaction before the recombination of electron and hole pairs.

In this work, a composite film composed of Ag, Al_2O_3 and TiO_2 was proposed. The Ag NPs were immersed in the host medium of Al_2O_3, and the TiO_2 film was sputtered on the Ag/Al_2O_3 film. A theoretical model for the radiant absorption of Ag/Al_2O_3-TiO_2 film was established based on Finite Difference Time Domain (FDTD) method [16]. The simulations were implemented by commercial FDTD package to analyze the effect of Ag NP radiant absorption on the composite film. The local radiant absorption of TiO_2 film in the Ag/Al_2O_3-TiO_2 composite film was also analyzed.

2. Radiant absorption model for Ag/Al_2O_3-TiO_2 composite film

The effect of Ag NPs on the TiO_2 film radiant absorption in the Ag/Al_2O_3-TiO_2 composite film is mainly related to the following factors: the Ag-TiO_2 distance and Ag NP size, distribution and morphology. The thicknesses of Al_2O_3 film and TiO_2 film could be controlled during the preparation and measured through ellipsometer method (Semilab R&D). The absorptance of the composite film was measured using an UV-VIS spectrophotometer (Evolution 220).

The radiant absorption model for Ag/Al_2O_3-TiO_2 composite film was established based on electromagnetic theory. The electromagnetic field in irradiated composite film could be described by Maxwell equations. The Finite Difference Time Domain (FDTD) method was applied to solve the equations. (see Supplementary Information Section S2). As the morphology, size and distribution of Ag NPs in the prepared composite films cannot be regulated precisely, the simulated results for the Al_2O_3-TiO_2 composite film without Ag NPs were compared with the measurable absorptance of the prepared Al_2O_3-TiO_2 films with the same layer thickness. The optical constants of Al_2O_3 film and TiO_2 films, which were needed for the simulation, were also investigated through ellipsometry

method (Semilab R&D). The measured and simulated data shown in Figure 1 were both transformed into the same unit. The FDTD model for Ag NPs was verified based on Mie theory (Figure 2). The results in Figure 2 were for the spherical Ag NPs with different radius *R* at the wavelength of 413.3 nm. The Relative Errors (RE) between them were calculated as follows:

$$\mathrm{RE} = \frac{x - \mu}{\mu} \times 100\% \tag{1}$$

where x is the simulated result, μ is the measured result or the result calculated from Mie theory.

The data in Figure 1 indicated that simulated results were close to the measured results. The data in Figure 1 indicated that the REs between simulated and measured results increased with the wavelength. The differences were probably due to measurement errors, the FDTD model's numerical error and the simplified Al_2O_3-TiO_2 interface structure in the simulated model. The data in Figure 2 indicated that the REs between the FDTD model and Mie theory increased with particle's Size Parameter. The differences could arise from numerical error.

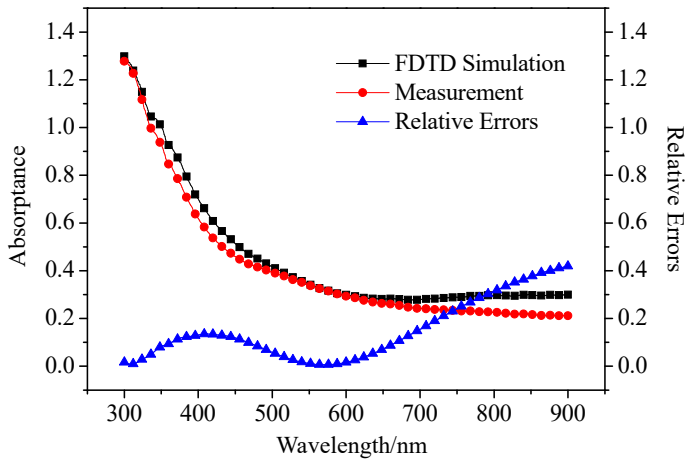

Figure 1. Comparison of measurable and simulated absorptance of Al_2O_3-TiO_2 composite film.

The model for analyzing the radiant absorption of the Ag/Al_2O_3-TiO_2 composite film was shown in Figure 3. The main objective of this work was to investigate the influence of Ag NPs on the radiant absorption of the Ag/Al_2O_3-TiO_2 composite film, especially on the radiant absorption of the TiO_2 film. A single layer of dispersed Ag NPs was assumed to be immersed in the host medium of Al_2O_3. The TiO_2 film with thickness of H_1 was located on the surface. Figure 3(a) presented a sectional view of Ag/Al_2O_3-TiO_2 composite film. H_2 was the distance between Ag and TiO_2. D was the diameter of Ag NPs, and L was the distance between two adjacent Ag NPs. The parameters and conditions of the model were set based on confirmation with experimental or analytical results, which were introduced at the beginning of this section. The unit cell for the FDTD modeling was sketched in Figure 3(b). The unite cell was periodic along the X and Y coordinate axes. The boundary conditions at the Z coordinate axis were set as the perfectly matched layer, which was an absorbing boundary. The incident source was set as a monochromatic plane wave propagating along the negative Z coordinate axis shown as an arrow in Figure 3(b). The incident polarization shown as a double-headed arrow in Figure 3(b) was along the X coordinate axis.

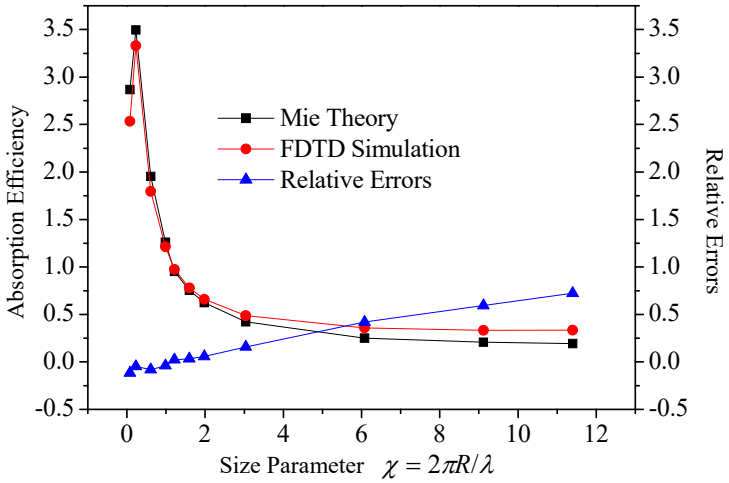

Figure 2. Comparison of FDTD model and Mie theory for the absorption efficiency (Q_{abs}) of Ag NPs, the complex refractive index is expressed as m = 0.226 + i 2.3, the wavelength is 413.3 nm.

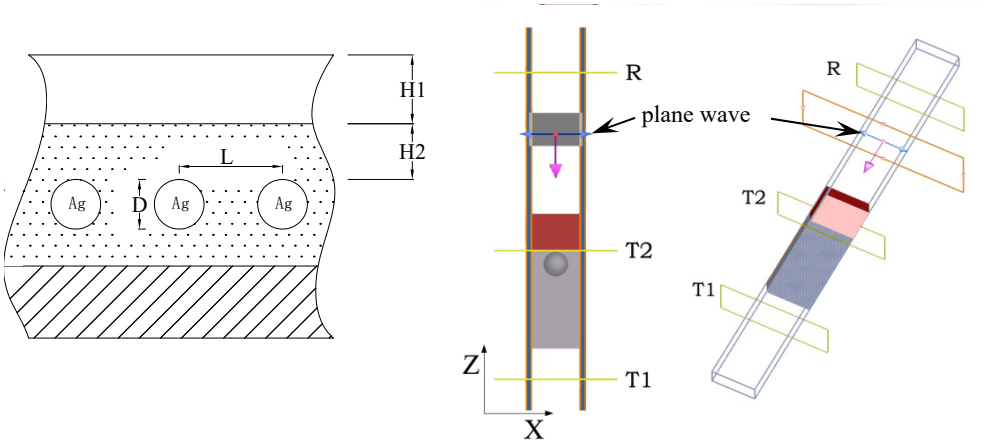

(a) Sectional view of Ag/Al_2O_3-TiO_2 composite film. (b) Sketched unit cell in the FDTD model.

Figure 3. Sketched model for the radiant absorption of Ag/Al_2O_3-TiO_2 composite film.

The radiant absorption model for the Ag/Al_2O_3-TiO_2 composite film was constructed based on electromagnetic theory (see Supplementary Information Section S2). The radiant absorption of Ag/Al_2O_3-TiO_2 composite film and TiO_2 film could be obtained using Eqs (2) and (3), respectively.

$$A_\lambda = 1 - r_\lambda - t_{1\lambda} \tag{2}$$

$$a_\lambda = 1 - r_\lambda - t_{2\lambda} \tag{3}$$

where A_λ was the spectral absorptivity of the Ag/Al_2O_3-TiO_2 composite film at the wavelength of

λ, r_λ was the spectral reflectivity gained in the plane R, $t_{1\lambda}$ was the spectral transmissivity gained in the plane T_1, a_λ was the spectral absorptivity of the TiO_2 layer in the composite film, and $t_{2\lambda}$ was the spectral transmissivity gained in the plane T_2.

3. Effect of Ag NPs on the radiant absorption of TiO_2 in the Ag/Al_2O_3-TiO_2 film

3.1. Influence of distance between Ag NPs and TiO_2

The influence of Ag-TiO_2 distance on the spectral absorptivity of Ag/Al_2O_3-TiO_2 composite film was analyzed using the radiant absorption model. The thickness (H_1) of the TiO_2 film was set as 60 nm. The distance (L) between two adjacent Ag NPs was set as 30nm. The diameter (D) of Ag NP was set as 20 nm. The distance (H_2) between Ag and TiO_2 was set at the value listed as "H_2-n" in Table 1. The Cases of TiO_2 film with the thickness of 60 nm and Ag/Al_2O_3 composite film without TiO_2 were also simulated. The results for the cases listed in Table 1 are compared in Figure 4, where Figure 4(a) shows the spectral absorptivity (A_λ) of Ag/Al_2O_3-TiO_2 composite film and Figure 4(b) shows the spectral absorptivity (a_λ) of the TiO_2 layer in the Ag/Al_2O_3-TiO_2 composite film. The radiant absorption of TiO_2 was intense in the short wavelength region. The value of the spectral absorptivity for the Ag/Al_2O_3-TiO_2 composite film decreased with the increasing wavelength. The main reason for this decline was the reduced absorption of the TiO_2 film. When the incident wavelength exceeded 300 nm, the effect of LSPR from Ag NPs became apparent. The spectral absorptivity for the Ag/Al_2O_3-TiO_2 composite film reached a small peak near 350 nm and the main peak near 530 nm. The value of spectral absorptivity increased with the increasing Ag-TiO_2 distance around the 350 nm peak and decreased with the increasing Ag-TiO_2 distance around the 530 nm peak. The influence of Ag-TiO_2 distance on the spectral absorptivity of the TiO_2 layer in Ag/Al_2O_3-TiO_2 composite film had the similar tendency as that shown in Figure 4(b).

However, the increased spectral absorptivity of the TiO_2 layer was considerably less than that of the Ag/Al_2O_3-TiO_2 composite film at the 350 nm peak and 530 nm peak mainly because the incident irradiation was highly localized at Ag NPs. Given that spectral absorptivity is proportional to the square of the local electric field in the composite film, the distribution of spectral absorptivity could be analyzed through the electric field maps. The maps in Figure 5 shows the internal relative electric-field intensity for Ag/Al_2O_3-TiO_2 composite film with the Ag-TiO_2 distance of 2 nm. The values shown in the maps are the internal electric-field intensity compared with incident electric-field intensity, which could be described by E/E_0. The internal electric field at the wavelengths below 387.5 nm can facilitate charge separation. The radiant absorption in the spectral range above 387.5 nm can generate heat in the composite film. Then temperature is increased in some localized regions, which may influence the photocatalytic performance. Based on these mechanisms, the internal electric field distributions at the two wavelengths of 550 nm and 370 nm were analyzed in Figure 5(a) and (b) respectively. The maps in Figure 5, which show the relative electric-field distribution in T_2 plane, indicate that the localized electric field in the TiO_2 cross section near the interface of TiO_2-Al_2O_3 could reach to 1.6 times the incident electric-field intensity at the wavelength of 550 nm and 0.78 times that at 370 nm. The simulated results for the case without Ag NPs showed that the maximum electric-field intensity in the T_2 plane was 0.616 times the incident electric-field intensity at wavelength of 550 nm and 0.651 times that at 370 nm. Incident radiation declined because of the absorption of TiO_2.

Table 1. Parameters for the simulations.

Cases	D/nm	L/nm	H_1/nm	H_2/nm
H_2-0 nm	20	30	60	0
H_2-2 nm	20	30	60	2
H_2-5 nm	20	30	60	5
H_2-10 nm	20	30	60	10
H_2-15 nm	20	30	60	15
H_2-20 nm	20	30	60	20
Al_2O_3-TiO_2	/	/	60	/
Ag/Al_2O_3	20	30	0	2

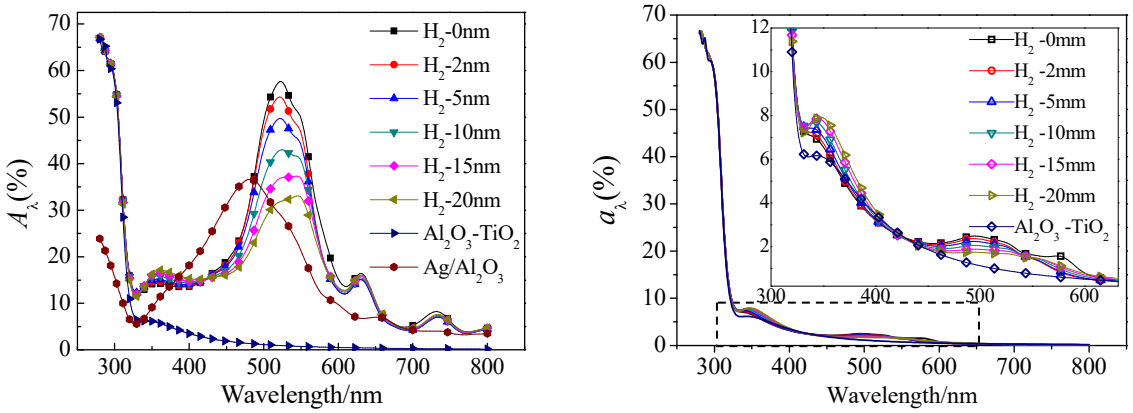

(a) Spectral absorptivity (A_λ) of Ag/Al_2O_3-TiO_2 composite film

(b) Spectral absorptivity (a_λ) of the TiO_2 layer in Ag/Al_2O_3-TiO_2 composite film

Figure 4. Influence of Ag-TiO_2 distance on the spectral absorptivity of Ag/Al_2O_3-TiO_2 composite film.

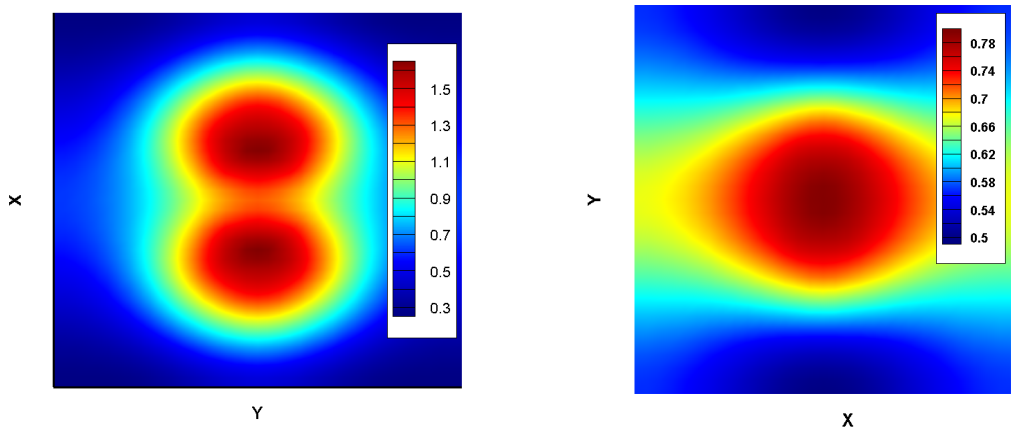

(a) The incident wavelength is 550 nm

(b) The incident wavelength is 370 nm

Figure 5. Relative electric-field intensity (E/E_0) in the T_2 plane of Ag/Al_2O_3-TiO_2 composite film with the Ag-TiO_2 distance of 2 nm.

The photocatalytic activities of the Ag/Al_2O_3-TiO_2 film, which were characterized based on their decomposition of methylene blue under the irradiation of HPMV, showed that the composite film with low Ag-TiO_2 distance possessed high catalytic activity (Supplementary Information). It was indicated that the generated electrons and holes in this composite film could be efficiently used for catalytic reaction. The simulated results presented in this section showed that the TiO_2 layer in the composite film with wide Ag-TiO_2 distance exhibited high spectral absorptivity in the incident wavelength region of 280 nm to 400 nm. Thus, the increased radiant absorption in the TiO_2 layer could not directly trigger the enhancement of the photocatalytic activity. Tuning the spots of the localized incident irradiation to the catalytic sites is important. Then the photocatalytic activity of the composite film is effectively enhanced. In the prepared composite film with low Ag-TiO_2 distance, the catalytic sites were close to the neighborhood of Ag NPs where the enhanced electric field was triggered. Thus, these composite films exhibited enhanced catalytic activities. The distribution of internal radiant absorption was needed to analyze for the optimal design of composite catalysts.

3.2. Influence of Ag NP morphology

In nanotechnology, many methods have been used to produce metal NPs, including chemical synthesis, light-induced rapid annealing et al, the NPs morphology can be modified by carefully controlling the synthetic condition. Then the metal NPs morphology can be optimized for their potential applications in plasmonic photocatalyst. In this part, the influence of Ag NP morphology was also analyzed through the constructed theoretical model sketched in Figure 4(b). Five different nanostructures considered for Ag NPs are shown in Figure 6. These nanostructures were spherical morphology, pyramid structure, cylinder, hollow cylinder (also called ring) and cube. The heights of these nanostructures were set at the same value of 40 nm. The underside of the pyramid structure was a square with the side-length of 40 nm. The underside of the cylinder was a circle with the radius of 40 nm. The underside of the hollow cylinder was a circular ring with the outside diameter of 40 nm and the inside diameter of 20 nm. The diameter of the sphere and the side-length of cube were both set at the value of 40 nm. The thickness H_1 of the TiO_2 film was set at 60 nm, and the distance H_2 between Ag and TiO_2 was 2 nm. Given that the distance L between two adjacent Ag NPs was 120 nm, so the interaction between the Ag NPs was sufficiently weak. Other parameters in this simulation were the same as those in section 3.2.2. The results for the five morphologies are compared in Figure 7, where Figure 7(a) shows the spectral absorptivity (A_λ) of the Ag/Al_2O_3-TiO_2 composite film, and Figure 7(b) shows the spectral absorptivity (a_λ) of the TiO_2 layer in the Ag/Al_2O_3-TiO_2 composite film. The radiant absorption of the TiO_2 layer played the main role in the wavelength reigon of 280~320 nm. Thus, the influence of Ag NPs morphology was not obvious in the wavelength region of 320~800 nm, the peaks of the composite films were located at different wavelengths because of the Ag NP morphology. The composite film with spherical Ag NPs had a main peak at 510 nm. The composite film with circular ring Ag NPs had a main peak at 650 nm and secondary peak at 360 nm. The spectral absorptivity of the composite film with cylindrical or cubic Ag NPs was also enhanced, and the peak wavelengths of the composite films with cylindrical and cubic Ag NPs were 575 nm and 630 nm respectively. The spectral absorptivity peak of the composite films with pyramidal Ag NPs was considerably less than those of other composite films in the wavelength region of 280~320 nm. The main reason for the result was the low absorptivity of pyramidal Ag NP under the irradiance from summit to underside of pyramidal Ag NP.

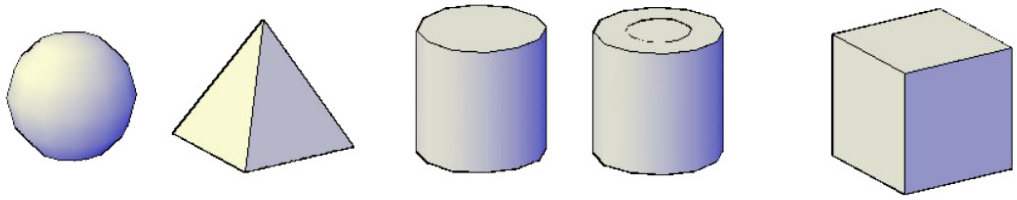

Figure 6. Five different morphologies of Ag NPs.

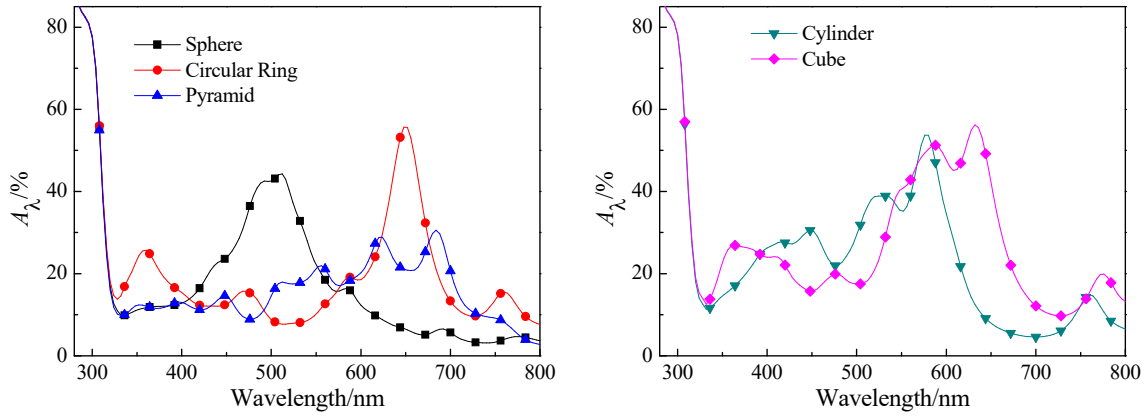

(a) Spectral absorptivity (A_λ) of Ag/Al_2O_3-TiO_2 composite film.

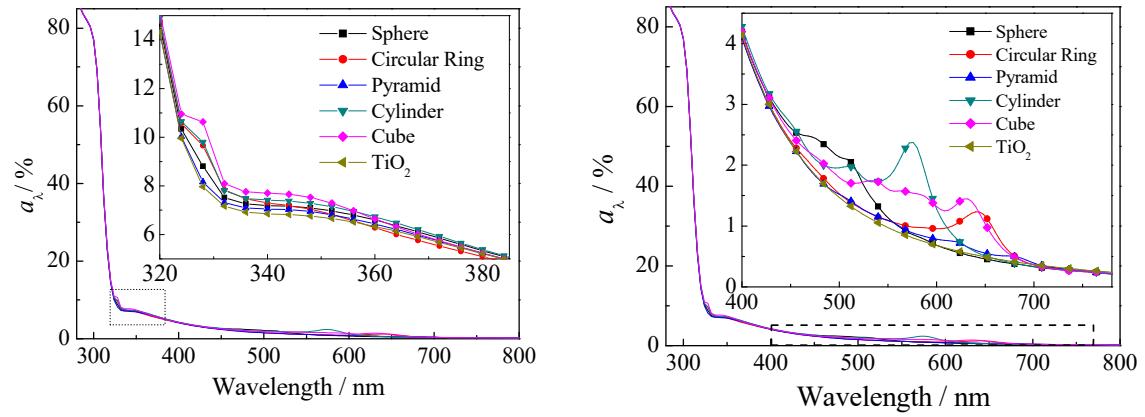

(b) Spectral absorptivity (a_λ) of TiO_2 layer in Ag/Al_2O_3-TiO_2 composite film.

Figure 7. Influences of Ag NP morphology on the spectral absorptivity of Ag/Al_2O_3-TiO_2 composite film.

The spectral absorptivity of TiO_2 layers in the composite film with and without Ag NPs are compared in Figure 7(b). In the wavelength region of 320~380 nm, the enhanced radiant absorption intensified because of the LSPR effect from Ag NPs. The plasmonic effect of Ag nanocube was stronger than that of the other samples in this wavelength region because of the secondary plasmonic

peak near 360 nm. When the wavelength was in the 400~700 nm region, the spectral absorptivity of the TiO_2 layer had the highest peak under the influence of cylindrical Ag NPs, and it had a wide enhanced region under the influence of cubic Ag NPs. The total effects of the five morphologies in the 400~700 nm region could be compared by using the following expression

$$f(i) = \sum_{n=400}^{700} (a_i(n) - a_T(n)) \tag{4}$$

where $a_i(n)$ was for spectral absorptivity of TiO_2 layers in the composite film with Ag NPs, subscript *i* represented each morphology, and $a_T(n)$ represented the spectral absorptivity of TiO_2 layers in the composite film without Ag NPs. The calculated results indicated that the plasmonic effect of Ag nanocylinders was stronger than that of the other samples in the wavelength region of 400–700 nm. The main reason for the result was the Ag nanocylinder enhanced radiant absorption in TiO_2 layer exist in a wider wavelength region.

Although the radiant absorption of the TiO_2 layer was considerably stronger below the wavelength of 330 nm, the incident radiation (e.g., solar irradiance) usually focused in the wavelength range from visible to near-infrared. The LSPR effect of Ag NPs was intense in the wavelength region of 400–700 nm. Thus, the electric field maps of the composite films were analyzed at the wavelength of main peak. The maps in the X-Z plane through the center of Ag NPs in Figure 8 showed the internal relative electric-field intensity for the composite film. The values in the maps also showed the internal electric-field intensity *E* compared with the incident electric-field intensity E_0. The electric field was highly enhanced around Ag NPs, especially near its angles. The relative electric-field intensity (E/E_0) could reach 70 in cylindrical Ag NPs. Given the highly localized internal electric field near the Ag NP surface, their distribution could not be identified in the TiO_2 layer as shown in Figure 8. The internal relative electric-field intensity maps in the TiO_2 layer are shown in Figure 9 at the peak wavelength, Figure 9(a) shows the X-Z section crossing the centers of Ag NPs and Figure 9(b) shows the X-Y cross section near the Al_2O_3-TiO_2 interface. The relative electric-field intensity in the TiO_2 layer was enhanced in different degrees and domains because of the difference in the Ag NP morphology. Among the five morphologies, Ag NPs with cylindrical morphology or hollow cylindrical morphology triggered wider and stronger internal radiant absorption in the TiO_2 layer. This is because most absorbed radiant energy in Ag NPs was localized near the surface with bigger curvature. In the composite films with cylindrical or hollow cylindrical Ag NPs, these localized regions were wider near TiO_2 layer.

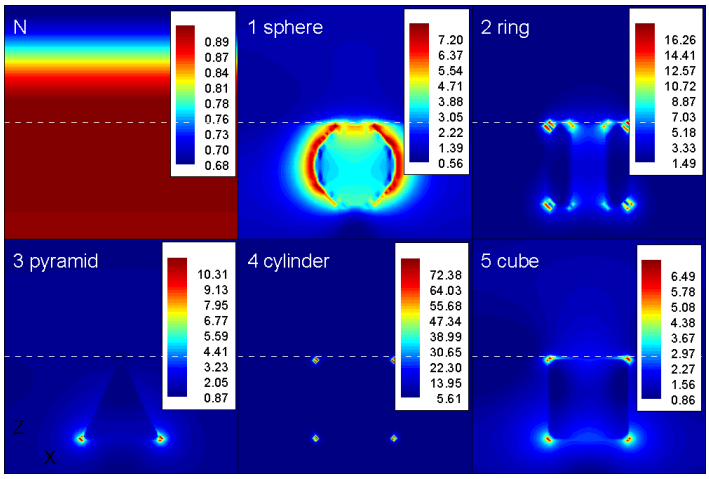

Figure 8. Relative electric-field intensity (E/E_0) of Ag/Al_2O_3-TiO_2 composite film with different Ag NP morphologies.

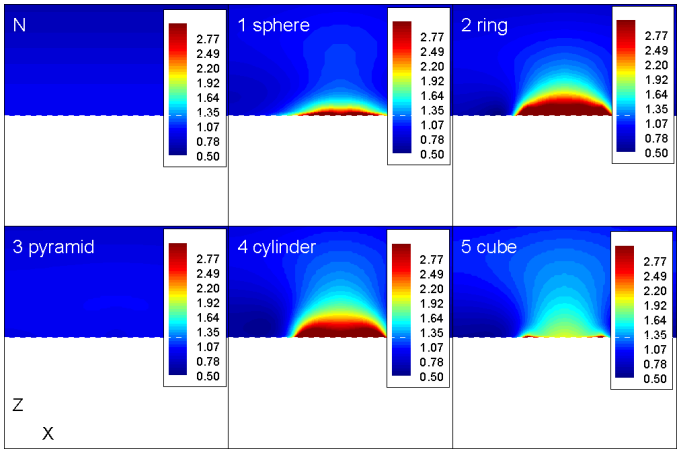

(a)

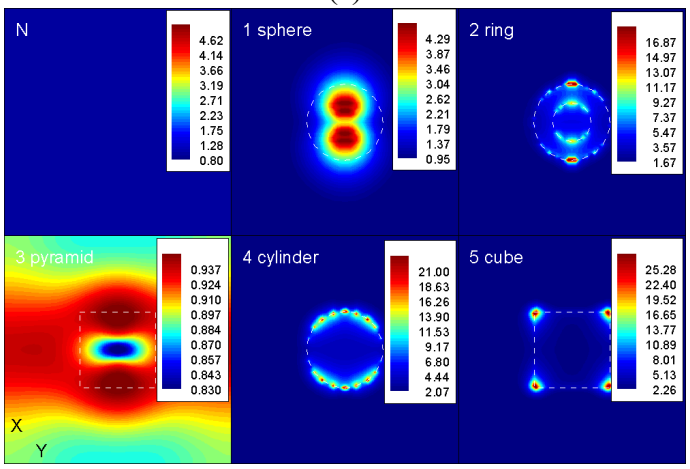

(b)

Figure 9. (a) Relative electric-field intensity (E/E_0) in the X-Z plane of the TiO_2 layer. (b) Relative electric-field intensity (E/E_0) in the X-Y plane of the TiO_2 layer near the Al_2O_3-TiO_2 interface.

4. Conclusions

The photocatalytic activity of TiO_2 film was promoted through combination with plasmonic Ag NPs. Al_2O_3 was proposed as the protective medium for Ag NPs. Thus, a thin layer of Al_2O_3 was placed between Ag NPs and the TiO_2 film. The degradation of aqueous methylene blue under the incident irradiation of HPMV indicated that the Ag/Al_2O_3-TiO_2 composite film with the Ag-TiO_2 distance of 2 nm or 5 nm exhibited high degradation rate. One possible reason for this phenomenon was that, in the composite film with low Ag-TiO_2 distance, the metal-semiconductor interface where photoinduced charge carriers were efficiently separated and the location where radiant absorption was localized were near the catalytic sites. The simulated results verified that the incident radiation was highly localized in the surrounding of Ag NPs.

The photocatalytic activity of Ag/Al_2O_3-TiO_2 composite film was related to several factors. This work was focused on the effect of Ag NPs on the radiant absorption of the photocatalyst film. The influences of Ag-TiO_2 distance and Ag NP morphology on the spectral absorptivity and radiant absorption distribution were systematically studied through FDTD simulation. The simulated results indicated that the nanostructure of the composite film could be regulated to an optimal case wherein spectral absorptivity and radiant absorption distribution were both beneficial to improve the photocatalytic activity.

Acknowledgment

This work was supported by National Natural Science Foundation of China (Grant No.51476078).

Conflict of interest

The authors declare that there are no conflict of interest in this paper.

Author contributions

Li Jiayu: Conceptualization, Methodology, Writing—review & Editing the manuscript, Funding acquisition. Guo Jiewen: Investigation, Modeling, Data analysis.

References

1. Jakob M, Levanon H, Kamat PV (2003) Charge Distribution between UV-Irradiated TiO_2 and gold nanoparticles: determination of shift in the Fermi level. *Nano Letters* 3: 353–358.
2. Subramanian V, Wolf EE, Kamat PV (2004) Catalysis with TiO_2/gold nanocomposites: Effect of metal particle size on the Fermi level equilibration. *J Am Chem Soc* 126: 4943–4950.
3. Awazu K, Fujimaki M, Rockstuhl C, et al. (2008) A plasmonic photocatalyst consisting of silver nanoparticles embedded in titanium dioxide. *J Am Chem Soc* 130: 1676–1680.
4. Sedghi M, Rahimi R, Rabbani M (2019) Design of a plasmonic photocatalyst structure consisting of metallic nanogratings for light-trapping enhancement. *Plasmonics* 14: 347–352.

5. Xie BW, Dong J, Zhao JM, et al. (2018) Radiative properties of hedgehog-like ZnO-Au composite particles with application to photocatalysis. *J Quant Spectrosc Ra* 217: 1–12.
6. Xie BW, Ma LX, Zhao JM, et al. (2019) Experimental study of the radiative properties of hedgehog-like ZnO-Au composite particles. *J Quant Spectrosc Ra* 232: 93–103.
7. Zhang LZ, Yu JC (2005) A simple approach to reactivate silver-coated titanium dioxide photocatalyst. *Catal Commun* 6: 684–687.
8. Romanyuk A, Oelhafen P (2007) Formation and electronic structure of TiO_2-Ag interface. *Sol Energy Mater Sol Cells* 91: 1051–1054.
9. Wang P, Huang BB, Dai Y, et al. (2012) Plasmonic photocatalysts: harvesting visible light with noble metal nanoparticles. *Phys Chem Chem Phys* 14: 9813–9825.
10. Chen X, Zhu HY, Zhao JC, et al. (2008) Visible-light-driven oxidation of organic contaminants in air with gold nanoparticle catalysts on oxide supports. *Angew Chem Int Ed* 47: 5353–5356.
11. Hu C, Peng TW, Hu XX, et al. (2010) Plasmon-induced photodegradation of toxic pollutants with Ag-AgI/Al_2O_3 under visible-light irradiation. *J Am Chem Soc* 132: 857–862.
12. Awadallah AE, Mostafa MS, Aboul-Enein AA, et al. (2014) Hydrogen production via methane decomposition over Al_2O_3-TiO_2 binary oxides supported Ni catalysts: effect of Ti content on the catalytic efficiency. *Fuel* 129: 68–77.
13. Ning XF, Zhen WL, Wu YQ, et al. (2018) Inhibition of CdS photocorrosion by Al_2O_3 shell for highly stable photocatalysts overall water splitting under visible light irradiation. *Appl Catal B: Environ* 226: 373–383.
14. Wang WC, Tsai MC, Yang J, et al. (2015) Efficiency enhancement of nanotextured black silicon solar cells using Al_2O_3/TiO_2 dual-layer passivation stack prepared by atomic layer deposition. *ACS Appl Mater Interfaces* 7: 10228–10237.
15. Li X, Liu PW, Mao Y, et al. (2015) Preparation of homogeneous nitrogen-doped mesoporous TiO_2 spheres with enhanced visible-light photocatalysis. *Appl Catal B: Environ* 164: 352–359.
16. Sullivan DM (2013) Electromagnetic simulation using the FDTD method, Second Edition, New York: John Wiley & Sons, 85–111.